ACS APPLIED MATERIALS & INTERFACES

Research Article

www.acsami.org

Polydopamine-Coated Magnetic Composite Particles with an Enhanced Photothermal Effect

Rui Zheng,[†] Sheng Wang,[‡,§] Ye Tian,[†] Xinguo Jiang,[‡] Deliang Fu,[§] Shun Shen,*[,‡] and Wuli Yang*[,†]

[†]State Key Laboratory of Molecular Engineering of Polymers and Department of Macromolecular Science, Fudan University, No. 220 Handan Road, Shanghai 200433, China

[‡]School of Pharmacy and Key Laboratory of Smart Drug Delivery, Fudan University, No. 826 Zhangheng Road, Shanghai 201203, China

[§]Pancreatic Disease Institute, Department of Pancreatic Surgery, Huashan Hospital, Shanghai Medical College, Fudan University, No. 12 Middle Urumqi Road, Shanghai 200040, China

Supporting Information

ABSTRACT: Recently, photothermal therapy (PTT) that utilizes photothermal conversion (PTC) agents to ablate cancer under near-infrared (NIR) irradiation has attracted a growing amount of attention because of its excellent therapeutic efficacy and improved target selectivity. Therefore, exploring novel PTC agents with an outstanding photothermal effect is a current research focus. Herein, we reported a polydopamine-coated magnetic composite particle with an enhanced PTC effect, which was synthesized simply through coating polydopamine (PDA) on the surface of magnetic Fe_3O_4 particles. Compared with magnetic Fe_3O_4 particles and PDA nanospheres, the core−shell nanomaterials exhibited an increased NIR absorption, and thus, an enhanced photothermal effect was obtained. We demonstrated the *in vitro* and *in vivo* effects of the photothermal therapy using our composite particles and their ability as a contrast agent in the T_2-weighted magnetic resonance imaging. These results indicated that the multifunctional composite particles with enhanced photothermal effect are superior to magnetic Fe_3O_4 particles and PDA nanospheres alone.

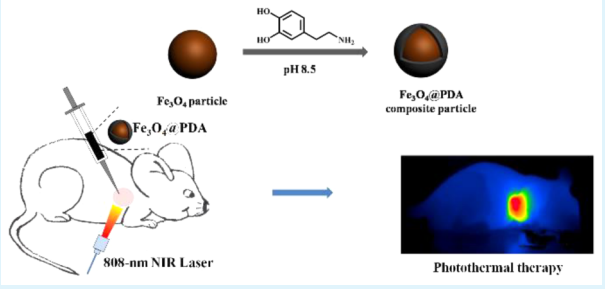

KEYWORDS: *composite particles, Fe_3O_4, polydopamine, tumor, photothermal therapy*

1. INTRODUCTION

Today, cancer is one of the main causes of death worldwide.[1,2] As cancer proliferates, many clinical cancer therapies have been developed, such as surgery, radiotherapy, and chemotherapy. However, these approaches suffer from the risks of killing normal cells and destroying the immune system.[3,4] Photothermal therapy (PTT), a minimally invasive local cancer treatment, has drawn great research and clinical attention during the past several years.[5] With a localized near-infrared (NIR) laser exposure, the photothermal conversion (PTC) agents can convert optical energy into heat to kill cancer cells locally, without the risk of destroying healthy tissues.[6,7] Recently, the PTC effects of many materials have been revealed, such as gold-based nanostructures,[8−13] carbon nanotubes,[14] graphene,[15,16] CuS nanocrystals,[17] polypyrrole,[18] and porphysome,[19] all of which exhibit strong optical absorbance in the NIR tissue optical transparency window.

Magnetic Fe_3O_4 particles, because of their magnetism and biocompatibility, have been widely used in biomedical research in the past decade. Research attention on Fe_3O_4 particles has been extensively focused on drug delivery, magnetic resonance imaging (MRI), biomarker detection, peptide enrichment and separation, etc.[20] Very recently, the photothermal effect of Fe_3O_4 particles (including clustered Fe_3O_4 particles and individual Fe_3O_4 nanocrystals) in the NIR region has been reported, and the particles have been used as a novel PTC agent in the photothermal ablation of tumors. Chu et al. first applied individual Fe_3O_4 nanocrystals at a high concentration for the PTT of cancer.[21] The Zhang group and our group further demonstrated that Fe_3O_4 superstructures exhibited a better photothermal effect with a significantly increased NIR absorption versus those of individual Fe_3O_4 nanocrystals.[22,23] The absorbance in the NIR region and photothermal conversion (PTC) efficiency are two key parameters that determine the efficacy of a PTC agent.[24] Because of the lower PTC efficiency of the clustered Fe_3O_4 particles, their absorbance in the NIR region is still inadequate for clinical applications in the field of cancer therapy.

Polydopamine (PDA), a mimic of the adhesive proteins found in the mussels, shows excellent biocompatibility and biodegradability.[25,26] PDA film could be easily deposited on many kinds of inorganic and organic materials, opening a new

Received: April 13, 2015
Accepted: July 7, 2015
Published: July 7, 2015

ACS Publications © 2015 American Chemical Society

DOI: 10.1021/acsami.5b03201
ACS Appl. Mater. Interfaces 2015, 7, 15876−15884

route to preparing functional materials for different applications.[27] Because of its strong NIR absorption and high PTC efficiency (40%), PDA has been recently utilized as an effective PTC agent in the research of PTT.[28] Lin et al. have modified PDA on the surface of individual Fe_3O_4 nanocrystals and applied the obtained nanocomposites for intracellular mRNA detection and imaging-guided PTT.[29]

In this work, we prepared magnetic composite particles with PDA coated on the clustered Fe_3O_4 particles and surprisingly revealed an enhanced photothermal effect of the composite particles, even better than that of pure PDA nanoparticles at an equivalent mass concentration. To the best of our knowledge, the enhanced photothermal effect of PDA-coated Fe_3O_4 particles (Fe_3O_4@PDA) has never been demonstrated. In the mechanistic study, the enhancement effect was proven to be a consequence of an increased NIR absorption after the PDA coating, for the PTC efficiency was still lower than that of PDA. On the basis of the outstanding photothermal effect, the *in vitro* and *in vivo* photothermal performances in a humanized orthotropic lung cancer model (A549) were investigated. After administration, they were able to ablate tumors effectively without damaging healthy tissues. Finally, the clustered Fe_3O_4 core also provides the composite particles with the ability to act as a contrast agent in the T_2-weighted MRI.

2. EXPERIMENTAL SECTION

2.1. Chemicals and Reagents. Iron(III) chloride ($FeCl_3{\cdot}6H_2O$), trisodium citrate dihydrate ($C_8H_5Na_3O_7{\cdot}2H_2O$), anhydrous sodium acetate (NaOAc), an aqueous ammonia solution ($NH_3{\cdot}H_2O$, 28–30%), ethanol, ethylene glycol (EG), and tris(hydroxymethyl)-aminomethane hydrochloride (Tris-HCl) were purchased from Shanghai Chemical Reagents Co. Dopamine hydrochloride (DA-HCl) was obtained from Aladdin Reagent Corp. (Shanghai, P. R. China). The MTT [3-(4,5-dimethylthiazol-2-yl)-2,5-diphenyltetrazolium bromide] assay and other biological reagents were purchased from Invitrogen Corp. Dulbecco's modified Eagle's medium (DMEM), fetal bovine serum (FBS), the penicillin/streptomycin solution, and the trypsin-EDTA solution were purchased from Gibco (Tulsa, OK). All the other chemicals were of analytical grade, and purified water was produced by a Millipore water purification system.

2.2. Synthesis of Clustered Fe_3O_4 Particles. The magnetic Fe_3O_4 particles were prepared by a modified solvothermal reaction.[30] Briefly, $C_8H_5Na_3O_7{\cdot}2H_2O$ (0.24 g), NaOAc (1.20 g), and $FeCl_3{\cdot}6H_2O$ (1.08 g) were first dissolved in EG (20 mL) while being mechanically stirred for 30 min. Then the resulting solution was transferred into a Teflon-lined stainless steel autoclave (with a volume of 50 mL). The autoclave was sealed and heated at 200 °C for 10 h and then cooled to room temperature. The obtained precipitate was washed with ethanol and deionized water several times and collected by magnetic separation. The final products were redispersed in ethanol (10 mL) for the following use.

2.3. Synthesis of Fe_3O_4@PDA Magnetic Composite Particles. The Fe_3O_4@PDA hybrid nanomaterials were synthesized by a solution oxidation method.[31] The as-prepared clustered Fe_3O_4 particles (25 mg) were dispersed in the Tris-HCl buffer solution (10 mM, pH 8.5, 500 mL). Then DA-HCl (125 mg) was added to the mixture described above. The resulting dispersion was continuously stirred for 1 h at room temperature. After the reaction, the precipitate was separated magnetically and washed with deionized water several times. The final products were dispersed in deionized water to obtain the desired Fe_3O_4@PDA particles. To tailor the thickness of the PDA shell, we altered the mass of clustered Fe_3O_4 particles while the mass of DA-HCl was fixed to 125 mg in the preparation process.

2.4. Synthesis of PDA Nanospheres. The PDA nanospheres with an average diameter of ~200 nm were prepared by the oxidation and self-polymerization of dopamine.[28] Briefly, 2 mL of an aqueous ammonia solution ($NH_3{\cdot}H_2O$, 28–30%) was mixed with 90 mL of deionized water and 40 mL of ethanol. Then the resulting solution was gently stirred for 0.5 h at 30 °C; 0.5 g of DA-HCl was dissolved in 10 mL of deionized water, and then it was injected into the mixture solution described above. Twenty-four hours later, the as-prepared PDA nanospheres were acquired by centrifugation and washed three times with deionized water.

2.5. Characterization. Transmission electron microscopy (TEM) images were observed on a Tecnai G2 20 TWIN transmission electron microscope (FEI). The hydrodynamic diameters and ζ potentials of particles were determined by a dynamic light scattering (DLS) particle size analyzer (Malvern Nano-ZS90) at a scattering angle of 90°. UV–vis spectra were recorded with a PerkinElmer Lambda 750 spectrophotometer at room temperature. Fourier transform infrared (FT-IR) spectra were recorded using KBr-pressed plates on a Nicolet 6700 FTIR spectroscope. Thermogravimetric analysis (TGA) was conducted on a Pyris 1 TGA instrument under an air environment at a heating rate of 20 °C min^{-1}. X-ray photoelectron spectroscopy (XPS) measurements were analyzed using an ESCA-Lab-200i-XL spectrometer with monochromatic Al Kα radiation (1486.6 eV). Magnetic property characterization was performed with a vibrating sample magnetometer (VSM) on a model 6000 physical property measurement system (Quantum) at 300 K. The X-ray diffraction (XRD) patterns were collected on an X'pert PRO diffractometer. Inductively coupled plasma atomic emission spectrometry (ICP-AES) was performed to determine the concentration of the Fe iron contents in the Fe_3O_4@PDA core–shell composite particles by a P-4010 spectrometer (Hitachi, Tokyo, Japan). T_2-weighted images of Fe_3O_4@PDA composite particles were obtained under a 3 T clinical MRI scanner (Magnetom Verio, Siemens).

2.6. NIR Heating Effect of Fe_3O_4, Fe_3O_4@PDA, and PDA in Dispersion. The as-prepared Fe_3O_4, Fe_3O_4@PDA, or PDA stock dispersion was diluted to 50 μg mL^{-1} and deposited into wells of a 96-well cell culture plate, with each well filled with 100 μL of the dispersion. Wells were illuminated by an 808 nm continuous-wave NIR laser (Changchun New Industries Optoelectronics Technology, Changchun, China; spot size of 6 mm × 7 mm) with laser irradiation at a power density of 6.6 W cm^{-2} for 500 s. Pre- and postillumination temperatures were measured by a thermocouple with an accuracy of 0.1 °C.

2.7. *In Vitro* Cell Assay. Human lung adenocarcinoma epithelial cells (A549 cells) were selected for the cell viability experiment. The cells (with a density of 10^4 cells per well) were incubated in a 96-well plates for 24 h to allow cell attachment. Then, the phosphate buffer solution (PBS), Fe_3O_4, PDA, and Fe_3O_4@PDA particles were added to the cells at the same concentration of 50 μg mL^{-1}. Afterward, the laser was applied to irradiate the cells at a power density of 6.6 W cm^{-2} from 0 to 180 s. An infrared camera thermographic system (InfraTec, VarioCAMhr research) was used to record the temperature of the dispersion in the plates. After further incubation for 24 h at 37 °C, the cells were incubated with MTT (0.5 mg mL^{-1}) in DMEM in the dark for an additional 4 h. Then they were mixed with dimethyl sulfoxide upon removal of the supernatant. The microplate reader (Synergy TM2, BIO-TEK Instruments Inc.) was applied to read the OD value at 570 nm, and the relative cell viability was determined by the percentage of the OD value of the study group over the control group.

2.8. *In Vivo* Photothermal Treatment. Male Balb/c mice (4–5 weeks of age and weighing ~20 g) were acquired from the Center of Experimental Animals of Fudan University. Animal care and handing procedures were in agreement with the guidelines evaluated and approved by the ethics committee of Fudan University. A549 subcutaneous tumors were inoculated by subcutaneous injection of 2 × 10^6 cells suspended in 100 μL of PBS into the flank region. The tumor size was monitored every week by a digital caliper. The tumor-bearing mice (with the longest dimension being ~5.0 mm) were randomized into four therapy groups (n = 5 per group): PBS with laser treatment (group I), Fe_3O_4 particles with laser treatment (group II), PDA nanospheres with laser treatment (group III), and Fe_3O_4@PDA composite particles with laser treatment (group IV). Each dispersion group at a concentration of 2 mg mL^{-1} was intratumorally injected into mice (injection volume of 25 μL). Two hours after injection, the

DOI: 10.1021/acsami.5b03201
ACS Appl. Mater. Interfaces 2015, 7, 15876–15884

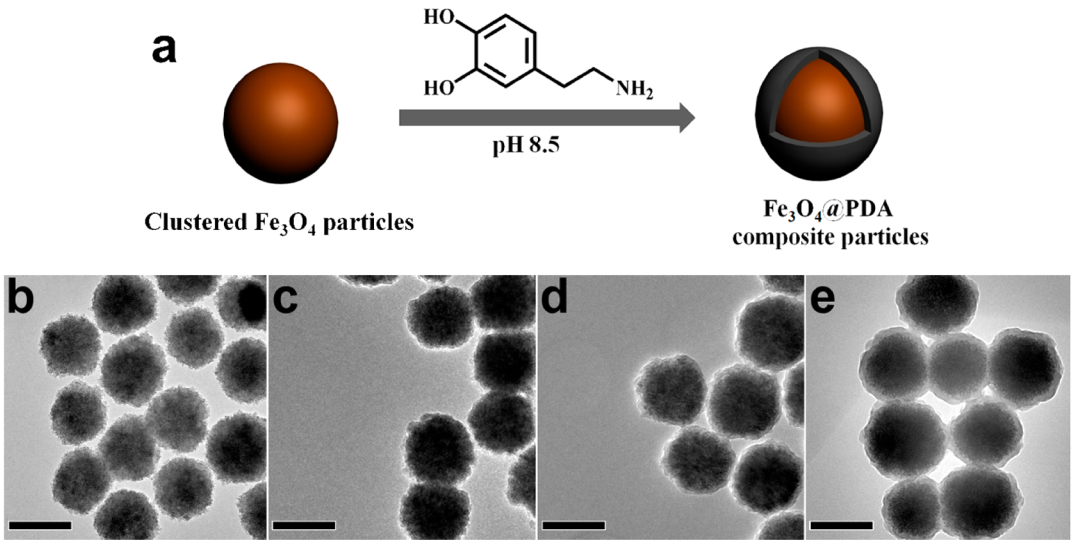

Figure 1. (a) Schematic illustration of the synthesis of Fe_3O_4@PDA composite particles. TEM images of clustered Fe_3O_4 particles (b) and Fe_3O_4@PDA composite particles with different PDA shell thicknesses [(c) Fe_3O_4@PDA-1, (d) Fe_3O_4@PDA-3, and (e) Fe_3O_4@PDA-5]. The bar is 200 nm.

tumors were exposed to the 808 nm NIR laser at a power density of 6.6 W cm^{-2} for 3 min. The tumor surface temperatures were recorded with an infrared camera thermographic system. The tumor sizes were measured by a caliper every other day. The tumor volume was calculated by the formula $V = {}^1/_2(LW^2)$, where L is the length (longest dimension) and W the width (shortest dimension). On day 19, all the mice were euthanized, and the tumors were dissected and weighed. Histological examination of the hematoxylin and eosin (H&E) stain assay was performed for the assessment of therapy efficacy.

2.9. Statistical Analysis. Statistical significance was determined by an unpaired Student's t test for two-group comparison and one-way analysis of variance with Fisher's LSD for multiple-group analysis. A P value of <0.05 was considered statistically significant. Results were expressed as means ± the standard deviation (SD) unless otherwise indicated.

3. RESULTS AND DISCUSSION

3.1. Preparation of Fe_3O_4@PDA Composite Particles. The solution oxidation method is the most widely used strategy for the production of PDA, such as coating various substrates with a uniform layer of a PDA film.[27] To synthesize Fe_3O_4@PDA composite particles, carboxyl group-functionalized clustered Fe_3O_4 particles were first prepared through a solvothermal reaction.[30] Because of the existence of carboxyl groups, dopamine could deposit on the surface of Fe_3O_4 particles by the formation of -$COO^-NH_3^+$- ion pairs and undergo self-polymerization under basic conditions to form a PDA shell with well-defined core−shell structures (Figure 1a).[26] In this preparation process, the thickness of the PDA shell could be controlled by adjusting the mass ratio of Fe_3O_4 particles and DA-HCl, and we altered the amount of Fe_3O_4 particles while the DA-HCl concentrations were fixed to 0.25 mg mL^{-1} in this work. Figure 1b−e shows the TEM images of the obtained Fe_3O_4 particles and the Fe_3O_4@PDA core−shell hybrid nanomaterials. It is very clear that both Fe_3O_4 and Fe_3O_4@PDA particles are well dispersed and spherical in shape. The Fe_3O_4 particles had an average diameter of ∼210 nm. The obtained Fe_3O_4@PDA particles with a dark Fe_3O_4 core were individually coated with gray PDA shells. After being coated with a PDA shell, the nanocomposites had a smooth surface. The mean thickness of the PDA coating shell was ∼7 nm [Fe_3O_4@PDA-1 (Figure 1c)] when the mass ratio of the Fe_3O_4 magnetic particles to DA-HCl is 1:1. While the mass ratio of the Fe_3O_4 magnetic particles to DA-HCl changed to 1:3 or 1:5, the average thickness of the PDA shell increased to ∼18 nm [Fe_3O_4@PDA-3 (Figure 1d)] or ∼27 nm [Fe_3O_4@PDA-5 (Figure 1e)]. The hydrodynamic diameter of the Fe_3O_4 particles was 245 nm (Table 1), which was close to the size measured by TEM, and the ζ potential was −46.8 mV for the existence of carboxyl groups on the surface of Fe_3O_4. After the samples had been coated with the PDA shell, the hydrodynamic diameters of the particles increased from 245 to ∼370 nm. In addition, the ζ potentials changed from −46.8 to ca. −25.0 mV because of the catechol groups on the surface of Fe_3O_4@PDA. Moreover, the polydispersity index (PDI) of Fe_3O_4@PDA was greater than that of Fe_3O_4, indicating that the dispersion stability of the particles decreased after PDA coating. The as-prepared Fe_3O_4@PDA particles could be stable in deionized water for ∼48 h.

Table 1. Particle Sizes and ζ Potentials of Fe_3O_4, Fe_3O_4@PDA-1, and Fe_3O_4@PDA-2[a]

sample	ζ potential (mV)	hydrodynamic diameter (nm)[b]	PDI[c]
Fe_3O_4	−46.8	245	0.05
Fe_3O_4@PDA-1[d]	−25.2	318	0.10
Fe_3O_4@PDA-2	−24.4	325	0.12
Fe_3O_4@PDA-3	−26.5	326	0.12
Fe_3O_4@PDA-4	−24.0	370	0.12
Fe_3O_4@PDA-5	−21.6	364	0.18

[a]All the data were measured at pH 7.4 in a 0.01 M phosphate buffer solution. [b]The diameter was determined at 25 °C by DLS. [c]PDI, polydispersity index. PDI = $\langle\mu_2\rangle/\Gamma^2$. [d]The number means the mass ratio of DA-HCl to Fe_3O_4 particles in the preparation procedure.

Figure 2a shows the FT-IR spectra of Fe_3O_4, Fe_3O_4@PDA, and PDA nanospheres. The band that appears at 580 cm^{-1} was related to the Fe−O vibration.[31] Compared with Fe_3O_4, the absorption peak at 1290 cm^{-1} appeared in the spectra of the Fe_3O_4@PDA and PDA nanospheres, which corresponded to the C−O stretching and primary amine vibration from PDA,[32] proving that the PDA shell had been successfully coated on the surface of Fe_3O_4. To quantitatively estimate the PDA coating

DOI: 10.1021/acsami.5b03201
ACS Appl. Mater. Interfaces 2015, 7, 15876−15884

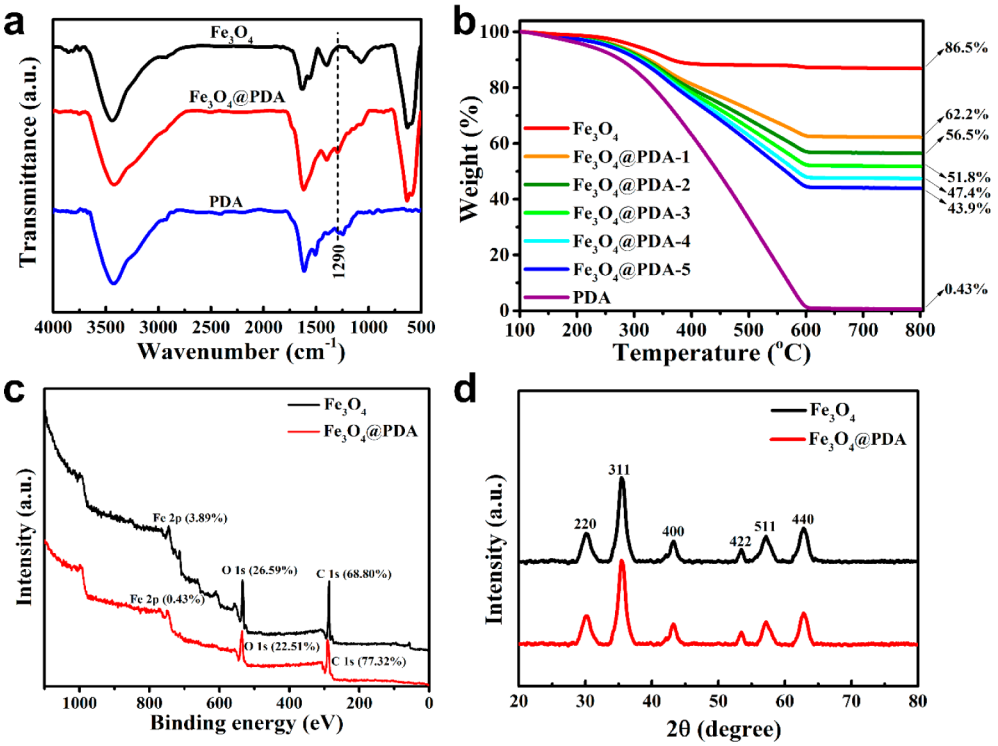

Figure 2. (a) FT-IR spectra of Fe_3O_4, PDA, and Fe_3O_4@PDA-5. (b) TGA curves of Fe_3O_4, PDA, and Fe_3O_4@PDA. (c) XPS spectra of Fe_3O_4 and Fe_3O_4@PDA-5. (d) XRD patterns of Fe_3O_4 and Fe_3O_4@PDA-5.

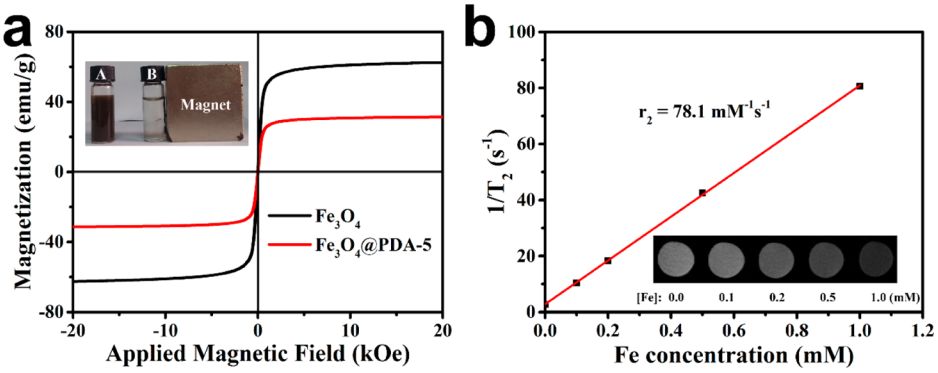

Figure 3. (a) Magnetic hysteresis curves of Fe_3O_4 and the Fe_3O_4@PDA-5 particles at 300 K. The inset photograph shows two bottles of the sample Fe_3O_4@PDA-5 composite particles in the same concentration of the aqueous solution, in which the particles were (A) well-dispersed in water and (B) attracted to the side wall by a magnet. After being gently shaken, the Fe_3O_4@PDA composite particles could be dispersed again in water. (b) T_2 relaxation rate of the Fe_3O_4@PDA-5 particles as a function of Fe concentration. The Fe concentration was determined by ICP-AES. The inset image shows T_2-weighted MRI photographs of the Fe_3O_4@PDA-5 particles dispersed in water at different Fe concentrations.

on the surface of Fe_3O_4, TGA of Fe_3O_4, Fe_3O_4@PDA, and PDA nanospheres was also conducted. As shown in Figure 2b, the weight loss was nearly 100 wt % for the PDA nanospheres in the heating process, and the weight loss was 13.5 wt % for Fe_3O_4 particles, caused by citrate groups on the surface, whereas the weight loss of Fe_3O_4@PDA-1 (37.8 wt %), Fe_3O_4@PDA-2 (43.5 wt %), Fe_3O_4@PDA-3 (48.2 wt %), Fe_3O_4@PDA-4 (52.6 wt %), and Fe_3O_4@PDA-5 (56.1 wt %) was mainly attributed to the PDA shell. Moreover, the weight loss of Fe_3O_4@PDA composite particles increased with an increase in PDA shell thickness.

To further confirm the PDA shell was triumphantly coated on the surface of the Fe_3O_4 particles, X-ray photoelectron spectroscopy (XPS) was conducted to provide detailed elemental information about the surface atomic composition of the obtained products. Figure 2c displays the XPS spectra of Fe_3O_4 and Fe_3O_4@PDA-5, which revealed the signals for C, O, Fe, and N elements. After the Fe_3O_4 particles were coated with a PDA shell, the percentage content for Fe decreased significantly from 3.89 to 0.43% while the percentage content for C increased from 68.80 to 77.32%. These results provided supportive evidence that the Fe_3O_4 cores were successfully coated with a shell of PDA. Figure 2d shows the XRD patterns of Fe_3O_4 and Fe_3O_4@PDA-5. All diffraction peaks in the black spectrum could be easily indexed and assigned to the typical cubic structure of Fe_3O_4 (JCPDS Card 75-1609). After PDA coating, the XRD patterns of Fe_3O_4@PDA (red) were similar to those of Fe_3O_4 (black), which indicated that the PDA shell did not change the crystalline phase of Fe_3O_4.

DOI: 10.1021/acsami.5b03201
ACS Appl. Mater. Interfaces 2015, 7, 15876−15884

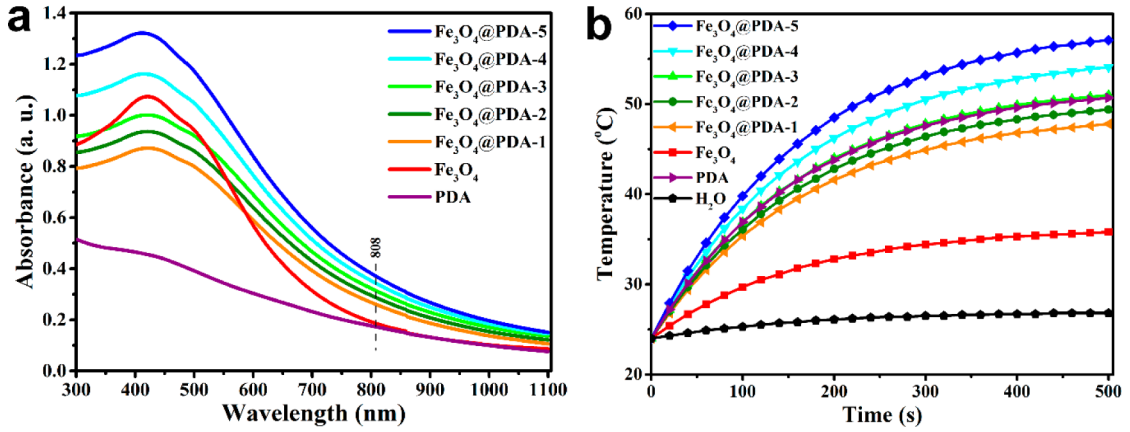

Figure 4. (a) UV−vis spectra of Fe_3O_4, PDA, and Fe_3O_4@PDA aqueous dispersions at a concentration of 50 μg mL^{-1}. (b) Photothermal effects of Fe_3O_4, PDA, and Fe_3O_4@PDA aqueous dispersions at a concentration of 50 μg mL^{-1} were measured by laser irradiation (λ = 808 nm; 6.6 W cm^{-2}) for 500 s.

The magnetic properties of Fe_3O_4 and Fe_3O_4@PDA were evaluated by a vibrating sample magnetometer (VSM). The magnetization curves (Figure 3a) implied that all the particles had no evident remanence or coercivity at 300 K, suggesting their superparamagnetic behaviors. The saturation magnetization (Ms) value of Fe_3O_4 particles was 62.4 emu g^{-1}. For Fe_3O_4@PDA composite particles with a thicker PDA shell, the Ms value of Fe_3O_4@PDA-5 was reduced to 31.2 emu g^{-1}. Although the Ms value of Fe_3O_4@PDA-5 decreased dramatically compared with that of the original Fe_3O_4 particles, the magnetism was still strong enough to facilitate their quick separation from solution within 30 s with the help of a magnet. Compared with the preparation process of the PDA nanospheres, which needed to spend much time during centrifugation for the collection of the products, it was very convenient and time-saving to separate the as-prepared Fe_3O_4@PDA from medium. Figure 3b shows the proton transverse relaxation rates ($1/T_2$) of the Fe_3O_4@PDA-5 dispersion as a function of iron concentration, and the r_2 value of Fe_3O_4@PDA-5 was calculated to be 78.1 mM^{-1} s^{-1}, lower than that of commercial MRI contrast agents (Resovist, 143 mM^{-1} s^{-1}; Feridex, 93 mM^{-1} s^{-1}).[33] The measured T_2-weighted MR images exhibited increasingly darker contrast with an increased Fe concentration. These results suggested the Fe_3O_4@PDA could be used as a promising contrast agent in MRI.

3.2. Photothermal Effect of Fe_3O_4@PDA Composite Particles. The absorbance intensity in the NIR region is one of the key factors that determine the PTC capability of a PTC agent. To explore how effective the nanomaterials could absorb light, their UV−vis spectra (at an equivalent concentration of 50 μg mL^{-1}) are summarized in Figure 4a. Fe_3O_4, Fe_3O_4@PDA, and PDA all had obvious absorption in the NIR region from 600 to 1000 nm. Compared with Fe_3O_4 and PDA, which had a similar absorption at 808 nm, Fe_3O_4@PDA presented a remarkable increase in NIR absorption at 808 nm at an equivalent mass concentration. Furthermore, the absorbance of Fe_3O_4@PDA particles increased with the increase in PDA shell thickness (Fe_3O_4@PDA-1 → Fe_3O_4@PDA-5). The strong optical absorption in the NIR region motivated us to investigate the photothermal effect of Fe_3O_4@PDA. The photothermal effects of Fe_3O_4, Fe_3O_4@PDA, and PDA were measured in water at 50 μg mL^{-1} irradiated with an 808 nm laser at 6.6 W cm^{-2} for 500 s. Pure water was used as a negative control. As seen from Figure 4b, the temperature of Fe_3O_4 dispersion was increased by 11.8 °C and significantly lower than that of PDA, which was increased by 26.7 °C. In contrast, the temperature of pure water was increased by only 2.8 °C. The temperature increased by Fe_3O_4@PDA dispersions could reach from 23.8 to 33.1 °C, much higher than that caused by Fe_3O_4. In addition, the temperatures were increased with an increasing PDA shell thickness (Fe_3O_4@PDA-1 → Fe_3O_4@PDA-5), indicating that the photothermal effect of Fe_3O_4@PDA could be improved by increasing the thickness of the PDA shell. Interestingly, when the shell of PDA was thick enough (Fe_3O_4@PDA-4 and Fe_3O_4@PDA-5), the photothermal effect of Fe_3O_4@PDA was much more efficient than that of PDA. Given another key factor that determines the PTC capability of a PTC agent, the photothermal conversion efficiencies of Fe_3O_4, PDA, and Fe_3O_4@PDA-5 particles were evaluated as follows.[34]

η is the photothermal conversion (PTC) efficiency, calculated using eq 1 described by Roper:

$$\eta = \frac{hS\Delta T_{max} - Q_s}{I(1 - 10^{-A_{808}})} \quad (1)$$

where h is the heat transfer coefficient, S is the surface area of the container, ΔT_{max} is the temperature change of the nanoparticles at the maximal steady-state temperature, Q_s is the heat associated with the NIR light absorbance of the solvent, I is the incident laser density (6.6 W cm^{-2}), and A_{808} is the absorbance of the nanoparticles at 808 nm.

The value of hS is derived according to eq 2:

$$\tau = \frac{m_s C_s}{hS} \quad (2)$$

where τ is the sample system time constant and m_s and C_s are the mass and the heat capacity of the solvent (pure water), respectively. According to eqs 1 and 2, the η value of Fe_3O_4@PDA-5 was calculated to be 13.1% (Figure S2b, Supporting Information), which was remarkably higher than that of Fe_3O_4 (6.4%) but lower than that of PDA (18.1%). The photothermal effect that shows how strongly a PTC agent can convert optical energy into heat depends on both PTC efficiency and the absorbance intensity in the NIR region.[22] Although Fe_3O_4@PDA-5 exhibited a PTC efficiency lower than that of PDA (Figure S2b, Supporting Information), they showed a higher absorbance value at 808 nm (Figure 3a), eventually resulting in

DOI: 10.1021/acsami.5b03201
ACS Appl. Mater. Interfaces 2015, 7, 15876−15884

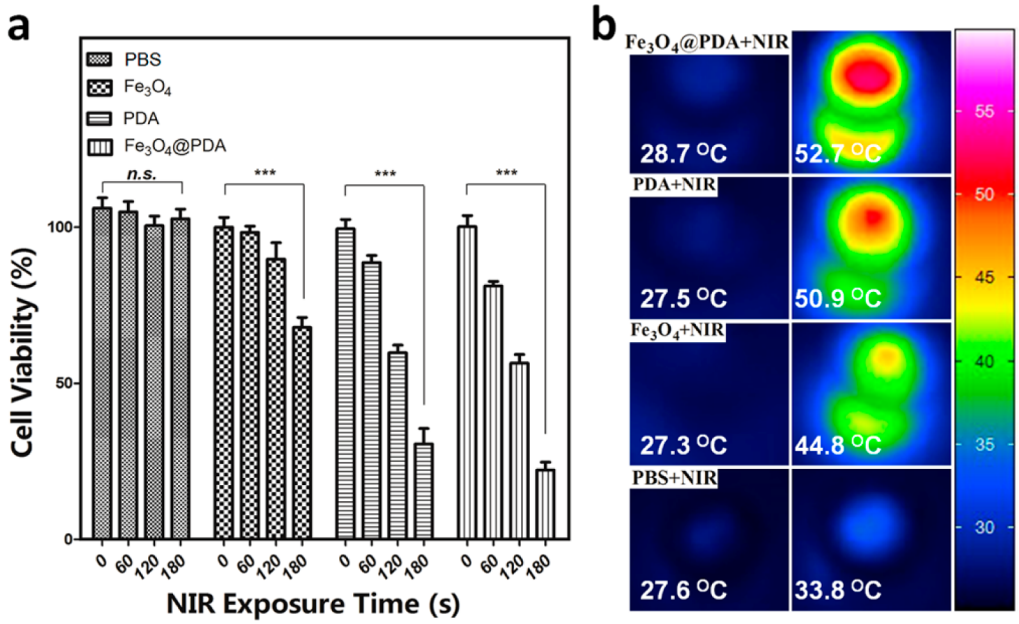

Figure 5. (a) Relative viabilities of A549 cells treated with Fe_3O_4, PDA, and Fe_3O_4@PDA at a concentration of 50 μg mL^{-1} without or with NIR laser irradiation (λ = 808 nm; 6.6 W cm^{-2}) for 0–180 s. (b) Temperatures of cells treated with Fe_3O_4, PDA, and Fe_3O_4@PDA recorded with an infrared camera thermographic system (left, before NIR irradiation; right, after NIR irradiation).

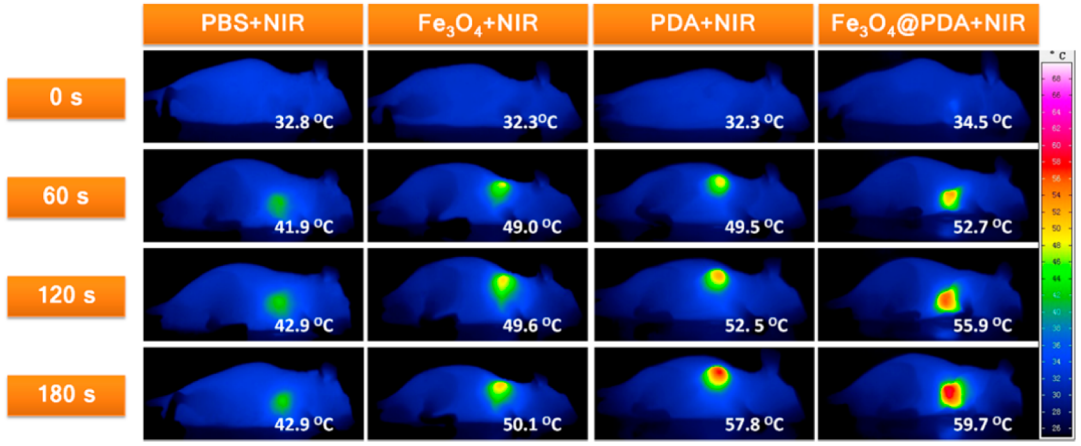

Figure 6. Infrared thermal images of Fe_3O_4, PDA, and Fe_3O_4@PDA with a dose of 50 μg of an injected A549 tumor sample under NIR laser irradiation (λ = 808 nm; 6.6 W cm^{-2}) for 0–180 s.

their photothermal effects being better than those of PDA at an equivalent concentration (50 μg mL^{-1}). These results revealed that the enhanced photothermal effect of Fe_3O_4@PDA particles was attributed to the increased NIR absorption rather than the PTC efficiency in our system.

Moreover, Fe_3O_4@PDA-5 aqueous dispersions at different concentrations (20, 50, 100, and 200 μg mL^{-1}) were chosen to further explore the impact of the concentration on the photothermal effect (Figure S3, Supporting Information). After continuous irradiation for 480 s, the temperature of the dispersions increased by 17.4–65.9 °C depending on the concentration of the Fe_3O_4@PDA-5 particles. Likewise, the temperature of the dispersions also increased with time, demonstrating that the NIR heating effect of Fe_3O_4@PDA was both time- and concentration-dependent. Because of the excellent enhanced photothermal effects, the Fe_3O_4@PDA composite particles with a thicker PDA shell (Fe_3O_4@PDA-5) were selected for further bioapplications *in vitro* and *in vivo*.

To examine the feasibility of Fe_3O_4, PDA, and Fe_3O_4@PDA in biomedicine, the nanomaterials were administered to A549 cells in 96-well plates, and each group was subdivided into groups with and without NIR laser exposure. The cytotoxic results are shown in Figure 5a. Almost no effect on cell viability was observed by direct irradiation of the cells because the low light absorption by natural endogenous cytochromes of these cells caused minimal temperature elevation that accounts for their high rate of survival.[6] Meanwhile, ~32.1% of cells were killed by Fe_3O_4 with a power density of 6.6 W cm^{-2} for 180 s at a concentration of 50 μg mL^{-1}. In contrast, ~69.4% of cells were killed at an equivalent concentration of 50 μg mL^{-1} for PDA, and ~77.8% of cells were killed by Fe_3O_4@PDA, meaning that A549 cells could be killed more efficiently by PDA and Fe_3O_4@PDA than by Fe_3O_4 with NIR laser exposure. The recorded temperature implied these nanomaterials were cytotoxic against A549 cells by NIR irradiation inducing hyperthermia (Figure 5b), which further demonstrated that

DOI: 10.1021/acsami.5b03201
ACS Appl. Mater. Interfaces 2015, 7, 15876–15884

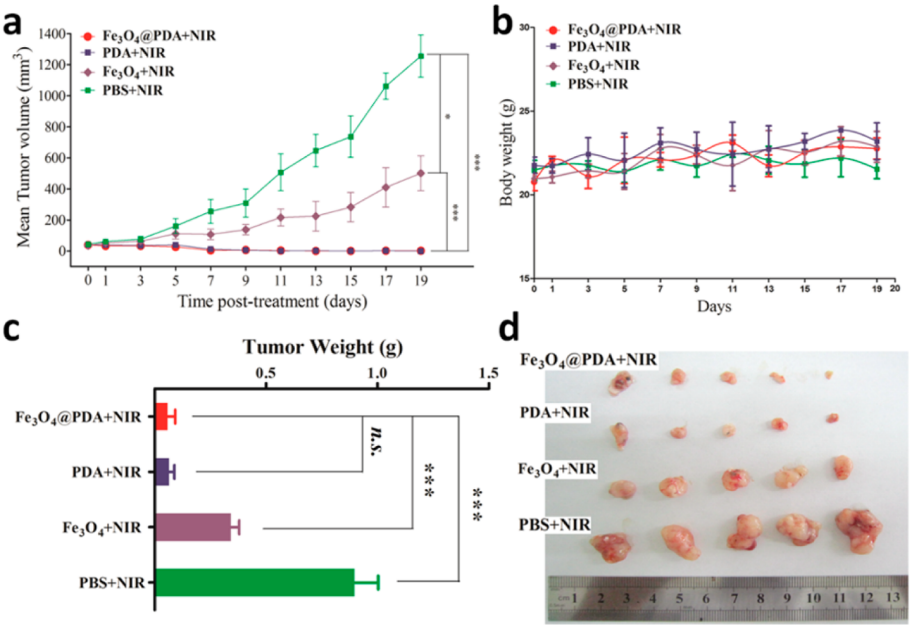

Figure 7. (a) Tumor growth curves of different groups after treatment. Tumor sizes were measured every 2 days. Means and standard errors are shown. (b) Body weight changes were recorded after therapy every 2 days. Means and standard errors are shown. (c) Tumor weights of each group. (d) Photograph of tumors after excision from PBS, Fe_3O_4, PDA, and Fe_3O_4@PDA under NIR irradiation. *n.s.* means no significant difference; $*P < 0.05$, and $***P < 0.001$.

Fe_3O_4@PDA composite particles exhibited an enhanced photothermal effect compared with Fe_3O_4 at an equivalent concentration. The inherent cytotoxicity of PDA and Fe_3O_4@PDA particles was also investigated. Their cell viabilities remained approximately 88.7 and 91.4%, respectively, when they were incubated with PDA and Fe_3O_4@PDA even at a high concentration of 400 μg mL^{-1} for 24 h (Figure S4, Supporting Information), confirming the lack of inherent toxicity of Fe_3O_4@PDA composite particles. The hemolysis experiment further demonstrated that the Fe_3O_4@PDA particles were nontoxic (Figure S5, Supporting Information).

3.3. Photothermal Therapy of Fe_3O_4@PDA *in Vivo*. We next performed *in vivo* PTT of Fe_3O_4, PDA, and Fe_3O_4@PDA. When the tumor reached approximately 5 mm in its longest dimension, Fe_3O_4, PDA, and Fe_3O_4@PDA particles with 25 μL of a treatment dispersion containing 50 μg were intratumorally administered to the tumor-bearing mice in groups II–IV, respectively. Laser irradiation was performed with an 808 nm NIR laser (6.6 W cm^{-2}; spot size, 6 mm × 7 mm; duration, 180 s) for every group. No mice died during the course of therapy. The tumor temperature changes on mice were recorded by an infrared camera thermographic system (Figure 6). In group II, the maximal temperature reached 50.1 °C in 180 s. In contrast, the temperature increase of the tumor surface for group I with injection of PBS was much less significant (only 42.9 °C after laser illumination for 180 s), showing that the NIR laser at such a power density could not induce sufficient heating by itself. The temperatures on the tumor surface from groups III and IV increased rapidly to 57.8 and 59.7 °C, respectively, which were higher than the temperature from group II. The results indicate Fe_3O_4@PDA nanomaterials exhibit the property of photothermal enhancement compared with Fe_3O_4 at an equivalent concentration. Moreover, in comparison with PDA nanospheres, the multifunctional Fe_3O_4@PDA particles could be used as MRI probes. MR imaging of A549 tumor-bearing mice was conducted after intratumoral injection of Fe_3O_4@PDA composite particles, revealing an obvious darkening effect with a T_2-MR signal decrease (Figure S6, Supporting Information).

Every 2 days, we measured the tumor sizes after diverse treatments (Figure 7a). The tumors of group I grew rapidly and reached 1255.3 mm^3 on day 19. Because of the photothermal effect of Fe_3O_4 particles, the tumors of group II grew relatively slowly and were reduced to 487.8 mm^3 in volume. The final tumor size exhibited a statistically significant difference ($P < 0.05$), which indicated that tumor growth was obviously affected by Fe_3O_4 particles with NIR irradiation for 180 s, which was consistent with our previous report.[22] At the same injection dose of particles, effects in groups III and IV were most pronounced. The tumors of groups III and IV were almost completely inhibited, and statistically significant tumor growth was observed in mice treated with PDA and Fe_3O_4@PDA particles and the NIR laser for 180 s ($P < 0.001$). During the photothermal treatment, the mice body weights of each group showed no obvious changes (Figure 7b). The mice photos of each group with different stages of treatment are presented in Figure S7 of the Supporting Information. Mice in treated groups III and IV were tumor-free by naked eyes after treatment. On day 19, mice were euthanized, and then tumors were excised and weighed (Figure 7c,d). The weights of tumors for groups I–IV were 0.8966 ± 0.1059, 0.3418 ± 0.0378, 0.0654 ± 0.0230, and 0.0582 ± 0.0338 g, respectively (Figure 7c). Remarkably, the antitumor efficiencies of groups III and IV were particularly prominent and were superior to those of all the other groups ($P < 0.001$). No statistically significant difference was observed in group III compared with group IV, indicating that the superior treatment effects were obtained with PDA and Fe_3O_4@PDA particles in the case of the same particles mass. Finally, the PTT effects were also assessed by histological analysis of H&E staining, which illustrated that the tumors in groups III and IV exhibited a scarlike structure containing numerous collagen bundles (Figure S8, Supporting Information). However, many tumor cells were observed in

DOI: 10.1021/acsami.5b03201
ACS Appl. Mater. Interfaces 2015, 7, 15876–15884

groups I and II. Therefore, the highly biocompatible Fe_3O_4@PDA particles showed an excellent enhanced photothermal effect compared with that of Fe_3O_4 particles at an equivalent concentration. Moreover, the Fe_3O_4 core also afforded the Fe_3O_4@PDA particles the ability to be used as a contrast agent in T_2-weighted MRI.

4. CONCLUSIONS

The enhanced NIR-absorbing multifunctional photothermal nanomaterials composed of a PDA shell and a magnetic particle core were prepared. The highly biocompatible Fe_3O_4@PDA composite particles showed an excellent enhanced photothermal effect compared with that of Fe_3O_4 particles at an equivalent concentration. In addition, both NIR absorption and the photothermal effect of Fe_3O_4@PDA particles increased with the increase in the thickness of the PDA shell. The enhanced photothermal effect of Fe_3O_4@PDA particles was attributed to increased NIR absorption, for Fe_3O_4@PDA exhibited a photothermal conversion efficiency lower than that of PDA. Greater cell killing was obtained when A549 cells incubated with Fe_3O_4@PDA particles were irradiated with NIR irradiation. A higher therapeutic efficacy was determined for *in vivo* tumor ablation by the NIR-induced hyperthermia of the Fe_3O_4@PDA composite particles. Moreover, Fe_3O_4@PDA composite particles were also applied as MRI probes for tumor diagnosis. Therefore, our research would be helpful for future clinical practices.

■ ASSOCIATED CONTENT

Supporting Information

Additional experimental details, including a TEM image of PDA nanospheres, the PTC efficiency of Fe_3O_4, Fe_3O_4@PDA-5, and PDA, the photothermal effects of Fe_3O_4@PDA-5 aqueous dispersions at different concentrations, the cytotoxicity of PDA and Fe_3O_4@PDA particles, hemolysis of Fe_3O_4@PDA, MR imaging, and H&E sections of tumors after treatment. The Supporting Information is available free of charge on the ACS Publications website at DOI: 10.1021/acsami.5b03201.

■ AUTHOR INFORMATION

Corresponding Authors

*Telephone: +86-21-65642385. Fax: +86-21-65640293. E-mail: wlyang@fudan.edu.cn.

*E-mail: sshen@fudan.edu.cn.

Author Contributions

R.Z. and S.W. contributed equally to this work.

Notes

The authors declare no competing financial interest.

■ ACKNOWLEDGMENTS

We thank the National Natural Science Foundation of China (Grants 51473037, 51273047, 81301974, and 81102847) and the "Shu Guang" project (12SG07) of Shanghai Municipal Education Commission and Shanghai Education Development Foundation for financial support.

■ REFERENCES

(1) Yoo, D.; Lee, J. H.; Shin, T. H.; Cheon, J. Theranostic Magnetic Nanoparticles. *Acc. Chem. Res.* **2011**, *44*, 863−874.

(2) Bardhan, R.; Lal, S.; Joshi, A.; Halas, N. J. Theranostic Nanoshells: From Probe Design to Imaging and Treatment of Cancer. *Acc. Chem. Res.* **2011**, *44*, 936−946.

(3) Kievit, F. M.; Zhang, M. Surface Engineering of Iron Oxide Nanoparticles for Targeted Cancer Therapy. *Acc. Chem. Res.* **2011**, *44*, 853−862.

(4) Vogel, A.; Venugopalan, V. Mechanisms of Pulsed Laser Ablation of Biological Tissues. *Chem. Rev.* **2003**, *103*, 577−644.

(5) Cheng, L.; Wang, C.; Feng, L.; Yang, K.; Liu, Z. Functional Nanomaterials for Phototherapies of Cancer. *Chem. Rev.* **2014**, *114*, 10869−10939.

(6) Shen, S.; Tang, H.; Zhang, X.; Ren, J.; Pang, Z.; Wang, D.; Gao, H.; Qian, Y.; Jiang, X.; Yang, W. Targeting Mesoporous Silica-Encapsulated Gold Nanorods for Chemo-Photothermal Therapy with Near-Infrared Radiation. *Biomaterials* **2013**, *34*, 3150−3158.

(7) Shen, S.; Ren, J.; Zhu, X.; Pang, Z.; Lu, X.; Deng, C.; Zhang, R.; Jiang, X. Monodisperse Magnetites Anchored onto Carbon Nanotubes: a Platform for Cell Imaging, Magnetic Manipulation and Enhanced Photothermal Treatment of Tumors. *J. Mater. Chem. B* **2013**, *1*, 1939−1946.

(8) Hleb, E. Y.; Hafner, J. H.; Myers, J. N.; Hanna, E. Y.; Rostro, B. C.; Zhdanok, S. A.; Lapotko, D. O. LANTCET: Elimination of Solid Tumor Cells with Photothermal Bubbles Generated around Clusters of Gold Nanoparticles. *Nanomedicine* **2008**, *3*, 647−667.

(9) Choi, W. I.; Kim, J. Y.; Kang, C.; Byeon, C. C.; Kim, Y. H.; Tae, G. Tumor Regression In Vivo by Photothermal Therapy Based on Gold-Nanorod-Loaded, Functional Nanocarriers. *ACS Nano* **2011**, *5*, 1995−2003.

(10) Loo, C.; Lowery, A.; Halas, N. J.; West, J.; Drezek, R. Immunotargeted Nanoshells for Integrated Cancer Imaging and Therapy. *Nano Lett.* **2005**, *5*, 709−711.

(11) Chen, J.; Wang, D.; Xi, J.; Au, L.; Siekkinen, A.; Warsen, A.; Li, Z. Y.; Zhang, H.; Xia, Y.; Li, X. Immuno Gold Nanocages with Tailored Optical Properties for Targeted Photothermal Destruction of Cancer Cells. *Nano Lett.* **2007**, *7*, 1318−1322.

(12) Lu, W.; Singh, A. K.; Khan, S. A.; Senapati, D.; Yu, H.; Ray, P. C. Gold Nano-Popcorn-Based Targeted Diagnosis, Nanotherapy Treatment, and In Situ Monitoring of Photothermal Therapy Response of Prostate Cancer Cells Using Surface-Enhanced Raman Spectroscopy. *J. Am. Chem. Soc.* **2010**, *132*, 18103−18114.

(13) Wang, Y.; Black, K. C. L.; Luehmann, H.; Li, W.; Zhang, Y.; Cai, X.; Wan, D.; Liu, S. Y.; Li, M.; Kim, P.; Li, Z. Y.; Wang, L. V.; Liu, Y.; Xia, Y. Comparison Study of Gold Nanohexapods, Nanorods, and Nanocages for Photothermal Cancer Treatment. *ACS Nano* **2013**, *7*, 2068−2077.

(14) Moon, H. K.; Lee, S. H.; Choi, H. C. In Vivo Near-Infrared Mediated Tumor Destruction by Photothermal Effect of Carbon Nanotubes. *ACS Nano* **2009**, *3*, 3707−3713.

(15) Yang, K.; Zhang, S.; Zhang, G.; Sun, X.; Lee, S. T.; Liu, Z. Graphene in Mice: Ultrahigh In Vivo Tumor Uptake and Efficient Photothermal Therapy. *Nano Lett.* **2010**, *10*, 3318−3323.

(16) Robinson, J. T.; Tabakman, S. M.; Liang, Y.; Wang, H.; Sanchez Casalongue, H.; Vinh, D.; Dai, H. Ultrasmall Reduced Graphene Oxide with High Near-Infrared Absorbance for Photothermal Therapy. *J. Am. Chem. Soc.* **2011**, *133*, 6825−6831.

(17) Li, Y.; Lu, W.; Huang, Q.; Huang, M.; Li, C.; Chen, W. Copper Sulfide Nanoparticles for Photothermal Ablation of Tumor Cells. *Nanomedicine* **2010**, *5*, 1161−1171.

(18) Yang, K.; Xu, H.; Cheng, L.; Sun, C.; Wang, J.; Liu, Z. In Vitro and In Vivo Near-Infrared Photothermal Therapy of Cancer Using Polypyrrole Organic Nanoparticles. *Adv. Mater.* **2012**, *24*, 5586−5592.

(19) Lovell, J. F.; Jin, C. S.; Huynh, E.; Jin, H.; Kim, C.; Rubinstein, J. L.; Chan, W. C. W.; Cao, W.; Wang, L. V.; Zheng, G. Porphysome Nanovesicles Generated by Porphyrin Bilayers for Use as Multimodal Biophotonic Contrast Agents. *Nat. Mater.* **2011**, *10*, 324−332.

(20) Guo, J.; Yang, W.; Wang, C. Magnetic Colloidal Supraparticles: Design, Fabrication and Biomedical Applications. *Adv. Mater.* **2013**, *25*, 5196−5214.

(21) Chu, M.; Shao, Y.; Peng, J.; Dai, X.; Li, H.; Wu, Q.; Shi, D. Near-Infrared Laser Light Mediated Cancer Therapy by Photothermal Effect of Fe_3O_4 Magnetic Nanoparticles. *Biomaterials* **2013**, *34*, 4078−4088.

DOI: 10.1021/acsami.5b03201
ACS Appl. Mater. Interfaces 2015, 7, 15876−15884

(22) Shen, S.; Wang, S.; Zheng, R.; Zhu, X.; Jiang, X.; Fu, D.; Yang, W. Magnetic Nanoparticle Clusters for Photothermal Therapy with Near-Infrared Irradiation. *Biomaterials* **2015**, *39*, 67−74.
(23) Zhang, X.; Xu, X.; Li, T.; Lin, M.; Lin, X.; Zhang, H.; Sun, H.; Yang, B. Composite Photothermal Platform of Polypyrrole-Enveloped Fe_3O_4 Nanoparticle Self-Assembled Superstructures. *ACS Appl. Mater. Interfaces* **2014**, *6*, 14552−14561.
(24) Huang, P.; Lin, J.; Li, W.; Rong, P.; Wang, Z.; Wang, S.; Wang, X.; Sun, X.; Aronova, M.; Niu, G.; Leapman, R. D.; Nie, Z.; Chen, X. Biodegradable Gold Nanovesicles with an Ultrastrong Plasmonic Coupling Effect for Photoacoustic Imaging and Photothermal Therapy. *Angew. Chem., Int. Ed.* **2013**, *52*, 13958−13964.
(25) Waite, J. H. Surface Chemistry - Mussel Power. *Nat. Mater.* **2008**, *7*, 8−9.
(26) Liu, Y.; Ai, K.; Lu, L. Polydopamine and Its Derivative Materials: Synthesis and Promising Applications in Energy, Environmental, and Biomedical Fields. *Chem. Rev.* **2014**, *114*, 5057−5115.
(27) Lee, H.; Dellatore, S. M.; Miller, W. M.; Messersmith, P. B. Mussel-Inspired Surface Chemistry for Multifunctional Coatings. *Science* **2007**, *318*, 426−430.
(28) Liu, Y.; Ai, K.; Liu, J.; Deng, M.; He, Y.; Lu, L. Dopamine-Melanin Colloidal Nanospheres: an Efficient Near-Infrared Photothermal Therapeutic Agent for In Vivo Cancer Therapy. *Adv. Mater.* **2013**, *25*, 1353−1359.
(29) Lin, L. S.; Cong, Z. X.; Cao, J. B.; Ke, K. M.; Peng, Q. L.; Gao, J.; Yang, H. H.; Liu, G.; Chen, X. Multifunctional Fe_3O_4@Polydopamine Core-Shell Nanocomposites for Intracellular mRNA Detection and Imaging-Guided Photothermal Therapy. *ACS Nano* **2014**, *8*, 3876−3883.
(30) Ma, W.; Xu, S.; Li, J.; Guo, J.; Lin, Y.; Wang, C. Hydrophilic Dual-Responsive Magnetite/PMAA Core/Shell Microspheres with High Magnetic Susceptibility and pH Sensitivity via Distillation - Precipitation Polymerization. *J. Polym. Sci., Part A: Polym. Chem.* **2011**, *49*, 2725−2733.
(31) Si, J.; Yang, H. Preparation and Characterization of Bio-Compatible Fe_3O_4@Polydopamine Spheres with Core/Shell Nanostructure. *Mater. Chem. Phys.* **2011**, *128*, 519−524.
(32) Sureshkumar, M.; Lee, C. K. Polydopamine Coated Magnetic-Chitin (MCT) Particles as a New Matrix for Enzyme Immobilization. *Carbohydr. Polym.* **2011**, *84*, 775−780.
(33) Rohrer, M.; Bauer, H.; Mintorovitch, J.; Requardt, M.; Weinmann, H. J. Comparison of Magnetic Properties of MRI Contrast Media Solutions at Different Magnetic Field Strengths. *Invest. Radiol.* **2005**, *40*, 715−24.
(34) Roper, D. K.; Ahn, W.; Hoepfner, M. Microscale Heat Transfer Transduced by Surface Plasmon Resonant Gold Nanoparticles. *J. Phys. Chem. C* **2007**, *111*, 3636−3641.

DOI: 10.1021/acsami.5b03201
ACS Appl. Mater. Interfaces 2015, 7, 15876−15884